Available online at www.sciencedirect.com
ScienceDirect
Journal of Computational Physics 227 (2008) 6448–6472
JOURNAL OF COMPUTATIONAL PHYSICS
www.elsevier.com/locate/jcp

Comparison between Lagrangian and mesoscopic Eulerian modelling approaches for inertial particles suspended in decaying isotropic turbulence

A. Kaufmann [a,*], M. Moreau [b], O. Simonin [b], J. Helie [b,1]

[a] CERFACS, 42 Av. G. Coriolis, 31057 Toulouse, France
[b] IMFT, UMR 5502 CNRS/INPT/UPS, Toulouse, France

Received 4 November 2006; received in revised form 2 March 2008; accepted 3 March 2008
Available online 14 March 2008

Abstract

The purpose of this paper is to evaluate the accuracy of the mesoscopic approach proposed by Février et al. [P. Février, O. Simonin, K.D. Squires, Partitioning of particle velocities in gas–solid turbulent flows into a continuous field and a spatially uncorrelated random distribution: theoretical formalism and numerical study, J. Fluid Mech. 533 (2005) 1–46] by comparison against the Lagrangian approach for the simulation of an ensemble of non-colliding particles suspended in a decaying homogeneous isotropic turbulence given by DNS. The mesoscopic Eulerian approach involves to solve equations for a few particle PDF moments: number density, mesoscopic velocity, and random uncorrelated kinetic energy (RUE), derived from particle flow ensemble averaging conditioned by the turbulent fluid flow realization. In addition, viscosity and diffusivity closure assumptions are used to compute the unknown higher order moments which represent the mesoscopic velocity and RUE transport by the uncorrelated velocity component. A detailed comparison between the two approaches is carried out for two different values of the Stokes number based on the initial fluid Kolmogorov time scale, $St_K = 0.17$ and 2.2. In order to perform reliable comparisons for the RUE local instantaneous distribution and for the mesoscopic kinetic energy spectrum, the error due to the computation method of mesoscopic quantities from Lagrangian simulation results is evaluated and minimized. A very good agreement is found between the mesoscopic Eulerian and Lagrangian predictions for the small particle Stokes number case corresponding to the smallest particle inertia. For larger particle inertia, a bulk viscous term is included in the mesoscopic velocity governing equation to avoid spurious spatial oscillation that may arise due to the inability of the numerical scheme to resolve sharp number density gradients. As a consequence, for $St_K = 2.2$, particle number density and RUE spatial distribution predicted by the mesoscopic Eulerian approach are more smooth with respect to the ones measured from the Lagrangian simulations results. Similarly, the Eulerian approach underestimates the mesoscopic kinetic energy for the high wavenumber modes while the agreement remains very good for the low wavenumber modes. For both cases, the mesoscopic Eulerian approach provides a good prediction of the time dependent particle and fluid-particle velocity correlations measured by spatial averaging in the whole computational domain.

* Corresponding author. Present address: Continental Mechanical Components GmbH, Regensburg, Germany. Tel.: +49 9405957702.
E-mail addresses: Andre.Kaufmann@siemens.com (A. Kaufmann), simonin@imft.fr (O. Simonin), Jerome.Helie@siemens.com (J. Helie).
[1] Present address: VDO Automotive, Toulouse, France.

0021-9991/$ - see front matter © 2008 Elsevier Inc. All rights reserved.
doi:10.1016/j.jcp.2008.03.004

Keywords: Particle laden flows; Eulerian methods; Preferential concentration; Compressibility

1. Introduction

Numerical simulation of particle laden flows using a Lagrangian approach, also called discrete particle simulation (DPS) approach, is a very powerful tool to study collective physical phenomena such as particle dispersion, preferential concentration, inter-particle collision, etc. Nevertheless, in real flows the full particle number cannot be accounted for and, usually, alternative approaches are needed to reduce the numerical cost. In such cases, the Eulerian treatment of the particulate phase may provide a convenient effective treatment. However, the derivation and closure of accurate local instantaneous Eulerian equations is still an open research subject. For example, Druzhinin and Elghobashi [2] derive Eulerian transport equation for the dispersed phase concentration and velocity by spatial averaging over a scale of the order of the Kolmogorov length scale, assumed to be larger than the particle diameter and inter-particle distance. In the frame of the equilibrium approach, the particle velocity can be written as a given algebraic function of the fluid velocity from a Taylor expansion of the particle velocity in terms of small particle response time to fluid characteristic time scale ratio. Validation of such an approach from DNS + DPS results was performed in homogeneous isotropic turbulence (HIT) [3] and homogeneous turbulent shear flow [4]. Though, a crucial assumption of the above approaches, the particle velocity uniqueness at a given position, fails when the particle relaxation time is larger than the Kolmogorov time scale, due to the crossing of particle trajectories.

To overcome this difficulty, Février et al. [1], proposed a probability density function (PDF) approach based on a conditional ensemble average of the particle properties for a given turbulent fluid flow realization. In such an approach, any discrete particle velocity may be separated into two contributions: an Eulerian velocity field, the mesoscopic velocity field (MVF) shared by all the particle realizations, and a Lagrangian random distribution, the random uncorrelated velocity (RUV), spatially uncorrelated and which accounts for the particle trajectory crossing. The conditional particle velocity PDF obeys a Boltzmann-type kinetic equation accounting for external forces acting on the particles and inter-particle collisions. The moments of the particle PDF are mesoscopic Eulerian quantities which obey transport equations derived by integration from the kinetic equation, following the same methodology as for the derivation of the Navier–Stokes equations in the frame of kinetic theory [5]. So, Février et al. [1] derived transport equations for particle number density, mesoscopic velocity, and random uncorrelated kinetic energy (RUE) and Simonin et al. [6] proposed, as a first approximation, a viscosity assumption to model the random uncorrelated kinetic stresses.

The mesoscopic approach was evaluated using a priori test from DPS coupled with DNS or LES of forced homogeneous isotropic turbulence [7] and fully developed channel flow [8]. In contrast, this study is the first attempt to solve the set of equations of the mesoscopic Eulerian approach allowing "a posteriori" quantitative comparison of the model predictions with reference results obtained from discrete particle simulation (DPS) coupled with DNS of an homogeneous isotropic decaying gaseous turbulence. In the present study, interaction forces are limited to Stokes drag and inter-particle collision effects are not taken into account. Particles are of identical size and the gravity force is not considered. However, the extension to evaporating droplets, gravity force and non-linear drag is not in conflict with the derivation methodology of the Eulerian field equations. Also the introduction of inter-particle collisions in dilute gas-particle mixture is without major difficulties [6]. The drastic assumptions are chosen in order not to focus this study on the effects related to particle turbulence dynamic interaction.

Comparisons between Eulerian and Lagrangian simulation results are performed considering several particle variables. First, Lagrangian statistical properties of the dispersed phase such as particle kinetic energy and particle-fluid velocity correlation are investigated. Second, local instantaneous mesoscopic Eulerian fields such as particle number density $\breve{n}_p$, mesoscopic velocity $\breve{u}_{p,i}$, and random uncorrelated kinetic energy $\delta\breve{\theta}_p$ fields are measured from both the Lagrangian and Eulerian simulations and compared. Finally, the mesoscopic particle kinetic energy spectra $E_p(k)$ computed from both Lagrangian and Eulerian simulation results are compared.

But to allow reliable comparisons between DPS and mesoscopic Eulerian simulation results an accurate spatial filtering procedure is needed to project Lagrangian quantities on a fixed grid and to compute the Eule-

rian fields (Fig. 1). To validate the proposed method, several projection methods are tested on a one-dimensional synthetic case. In the case of non-interacting particles, the number of particles per cell for a given carrier phase realization is not limited, a Gaussian projector is then validated from the kinetic energy spectrum using DPS results with different simulated particle numbers.

The paper is organised as follow: the mesoscopic Eulerian approach is presented in Section 2, then the projection method to compute mesoscopic Eulerian field from DPS results is described and validated in Section 3, Section 4 concerns the numerical test case description, finally Eulerian simulation predictions are presented and compared with DPS results in Section 5.

2. The mesoscopic Eulerian approach

To derive local instantaneous particle Eulerian equations in dilute flows (without turbulence modification by the particles), Février et al. [1,7,6] introduce an ensemble average over dispersed phase realizations $\langle\cdot\rangle$ conditioned by any given carrier phase realization. Such an averaging procedure leads to a conditional particle velocity PDF $\breve{f}_{\mathrm{p}}^{(1)}(\mathbf{c}_{\mathrm{p}};\mathbf{x},t|H_{\mathrm{f}})$,

$$\breve{f}_{\mathrm{p}}^{(1)}(\mathbf{c}_{\mathrm{p}},\mathbf{x},t;H_{\mathrm{f}}) = \langle W_{\mathrm{p}}^{(1)}(\mathbf{c}_{\mathrm{p}},\mathbf{x},t)|H_{\mathrm{f}}\rangle \tag{1}$$

$W_{\mathrm{p}}^{(1)}$ is the fine grid PDF of the realizations of position and velocity in time of any given particle [9] and H_{f} represents the given carrier fluid flow realization. This function represents the local instantaneous probable number density of particles with a translation velocity $\mathbf{u}_{\mathrm{p}} = \mathbf{c}_{\mathrm{p}}$ at the location $\mathbf{x}$ for a given time t. The conditional PDF obeys a Boltzmann-type kinetic equation, which accounts for momentum exchange with the carrier fluid, gravity force, and particle–particle collisions. Thus, neglecting the collision effect, the conditional PDF equation takes the form:

$$\frac{\partial}{\partial t}\breve{f}_{\mathrm{p}} + \frac{\partial}{\partial x_j}c_{\mathrm{p},j}\breve{f}_{\mathrm{p}} + \frac{\partial}{\partial c_{\mathrm{p},j}}\left[\frac{F_{\mathrm{p},j}}{m_{\mathrm{p}}}\breve{f}_{\mathrm{p}}\right] = 0 \tag{2}$$

The PDF equation can be used to derive transport equations for the moments (number density $\breve{n}_{\mathrm{p}}$, mesoscopic velocity $\breve{u}_{\mathrm{p}}$, ...) of the dispersed phase following kinetic theory methodology [5].

2.1. Transport equations for particle properties

Instead of resolving directly the Boltzmann-type kinetic equation (2) one may compute only some first order moments of the particle velocity PDF from separate Eulerian transport equations with constitutive relations for the unknown needed higher order moments. Such a approach is a transposition of the classical

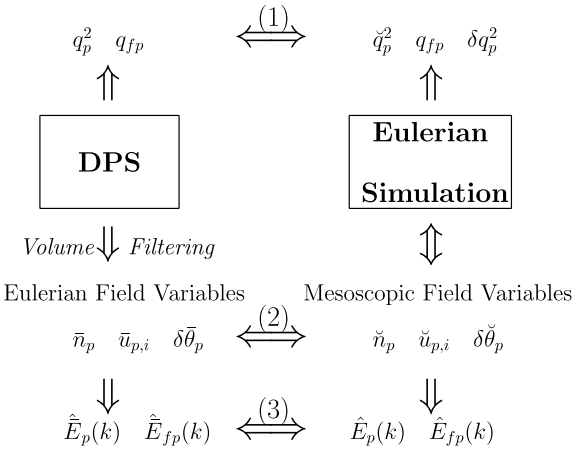

Fig. 1. Methodology for comparison of DPS to Eulerian simulation approaches.

kinetic theory moment method for dilute gases which involves the computation of the density, velocity and temperature using the Navier–Stokes and energy transport equations. So, integration over the particle velocity phase space yields statistical "mesoscopic" properties of the dispersed phase. The "mesoscopic" particle number density is written as

$$\breve{n}_{\mathrm{p}} = \int \breve{f}_{\mathrm{p}}^{(1)}(\mathbf{c}_{\mathrm{p}}, \mathbf{x}, t; H_{\mathrm{f}})\, \mathrm{d}\mathbf{c}_{\mathrm{p}} \tag{3}$$

All the mesoscopic moments of the dispersed phase are obtained by integration of velocity component polynomials, $\Phi(\mathbf{c}_{\mathrm{p}}) = c_{\mathrm{p},i}^{a} c_{\mathrm{p},j}^{b} c_{\mathrm{p},k}^{c} \cdots$, multiplied by the conditional PDF:

$$\breve{\Phi} = \langle \Phi | H_f \rangle_{\mathrm{p}} = \frac{1}{\breve{n}_{\mathrm{p}}} \int \Phi(\mathbf{c}_{\mathrm{p}}) \breve{f}_{\mathrm{p}}^{(1)}(\mathbf{c}_{\mathrm{p}}, \mathbf{x}, t; H_{\mathrm{f}})\, \mathrm{d}\mathbf{c}_{\mathrm{p}} \tag{4}$$

With this definition one may define a local instantaneous particulate velocity field, which is here named mesoscopic Eulerian particle velocity field

$$\breve{\mathbf{u}}_{\mathrm{p}}(\mathbf{x}, t; H_{\mathrm{f}}) = \frac{1}{\breve{n}_{\mathrm{p}}} \int \mathbf{c}_{\mathrm{p}} \breve{f}_{\mathrm{p}}^{(1)}(\mathbf{c}_{\mathrm{p}}, \mathbf{x}, t; H_{\mathrm{f}})\, \mathrm{d}\mathbf{c}_{\mathrm{p}} \tag{5}$$

For simplicity, the dependence of the above variables on the single carrier phase realization H_{f} is not written explicitly further in the paper. Then, the velocity of any discrete particle $u_{\mathrm{p},i}^{(k)}$ can be decomposed in the local instantaneous mesoscopic Eulerian velocity at the particle position $\breve{u}_{\mathrm{p},i}$ and a Lagrangian component $\delta u_{\mathrm{p},i}^{(k)}$:

$$u_{\mathrm{p},i}^{(k)}(t) = \breve{u}_{\mathrm{p},i}(\mathbf{x}_{\mathrm{p}}^{(k)}(t), t) + \delta u_{\mathrm{p},i}^{(k)}(t) \tag{6}$$

The Lagrangian component $\delta u_{\mathrm{p},i}^{(k)}$ of the discrete particle velocity is referred as the random spatially uncorrelated velocity (RUV)[2] component. Indeed, as shown by Février et al. [1], $\delta u_{\mathrm{p},i}^{(k)}$ between any two different particles are uncorrelated, therefore the two-point particle velocity correlation,

$$\delta R_{\mathrm{p},ij}(\mathbf{x}, \mathbf{x}') = 0 \quad \forall(\mathbf{x}, \mathbf{x}') \quad \text{if } |\mathbf{x} - \mathbf{x}'| > 0 \tag{7}$$

where

$$\delta R_{\mathrm{p},ij}(\mathbf{x}, \mathbf{x}') = \iint [c_{\mathrm{p},i} - \breve{u}_{\mathrm{p},i}(\mathbf{x}, t)][c'_{\mathrm{p},j} - \breve{u}_{\mathrm{p},j}(\mathbf{x}', t)] \breve{f}_{\mathrm{p}}^{(2)}(\mathbf{c}_{\mathrm{p}}, \mathbf{c}'_{\mathrm{p}}, \mathbf{x}, \mathbf{x}', t; H_{\mathrm{f}})\, \mathrm{d}\mathbf{c}_{\mathrm{p}}\, \mathrm{d}\mathbf{c}'_{\mathrm{p}} \tag{8}$$

This uncorrelated Lagrangian velocity distribution is similar to the peculiar velocity distribution in the framework of kinetic theory of dilute gases which obeys the molecular chaos assumption. Nevertheless it has to be pointed out that the particle position distribution is not as random due to the segregation mechanism and the uncorrelated velocity distribution is not Gaussian.

Using standard kinetic theory method [5], transport equations of particle number density and mesoscopic Eulerian velocity are derived by integration of the Boltzmann-type equation (2) over the particle velocity space:

$$\frac{\partial}{\partial t} \breve{n}_{\mathrm{p}} + \frac{\partial}{\partial x_i} \breve{n}_{\mathrm{p}} \breve{u}_{\mathrm{p},i} = 0 \tag{9}$$

$$\breve{n}_{\mathrm{p}} \frac{\partial}{\partial t} \breve{u}_{\mathrm{p},i} + \breve{n}_{\mathrm{p}} \breve{u}_{\mathrm{p},j} \frac{\partial}{\partial x_j} \breve{u}_{\mathrm{p},i} = -\frac{\breve{n}_{\mathrm{p}}}{\tau_{\mathrm{p}}} [\breve{u}_{\mathrm{p},i} - u_{f,i}] + \frac{\partial}{\partial x_j} \breve{n}_{\mathrm{p}} \delta \breve{\sigma}_{\mathrm{p},ij} \tag{10}$$

where the first term on the right hand side of Eq. (10) represents the drag force, with $u_{\mathrm{f},i}$ the carrier phase velocity at the particle position. τ_{p} is the particle relaxation time modelled using Stokes drag:

$$\tau_{\mathrm{p}} = \frac{\rho_{\mathrm{p}} d^2}{18 \mu_{\mathrm{f}}} \tag{11}$$

[2] *Random spatially uncorrelated velocity* (*RUV*) has been referred to as *Quasi Brownian Motion* (*QBM*) in previous publications. We agree that the expression *Quasi Brownian* is misleading since the physical interpretation of the uncorrelated motion is not of *Brownian* nature.

Here ρ_p is the density of the particle, d is the particle diameter and μ_f is the dynamic viscosity of the carrier phase. The stress term in Eq. (10) arises from the integration of the convective term in the PDF transport equation (2):

$$\breve{n}_p \delta\breve{\sigma}_{p,ij} = -\int (c_{p,i} - \breve{u}_{p,i})(c_{p,j} - \breve{u}_{p,j}) \breve{f}_p^{(1)}(\mathbf{c}_p, \mathbf{x}, t; H_f)\, d\mathbf{c}_p \tag{12}$$

$$= -\breve{n}_p \langle \delta u_{p,i} \delta u_{p,j} | H_f \rangle_p \tag{13}$$

This term account for the transport of mesoscopic momentum due to the uncorrelated part of the particle velocity.

The time dependent fields of the particle number density and mesoscopic velocity can be predicted using Eqs. (9) and (10). It is however necessary to model the second-order particle PDF moments, or RUV kinetic stress tensor, $\delta\breve{\sigma}_{p,ij}$ in terms of computed variables. One possibility is to solve separate transport equations for the components of the RUV kinetic stress tensor. Such equations can be derived from the PDF equation but this method shifts the difficulty in finding constitutive relations for the third-order particle PDF moments, or triple RUV correlations, and increases drastically the numerical cost by solving six additional transport equations. Alternatively, one can try to model directly the second-order RUV correlations using computed mesoscopic variables as performed in the frame of kinetic theory of dilute gases when writing the viscosity assumption in the Navier–Stokes equation.

2.2. Random uncorrelated velocity (RUV) correlation tensor modelling

When the Euler or Navier–Stokes equations are derived from kinetic gas theory, the trace of $\langle \delta u_{p,i} \delta u_{p,j} \rangle_p$ is interpreted as temperature (ignoring the Boltzmann constant and molecular mass) and defined as the uncorrelated part of the molecular kinetic energy. By analogy, the random uncorrelated particle kinetic energy (RUE) is defined as half the trace of $\delta\breve{\sigma}_{p,ij}$:

$$\delta\breve{\theta}_p = \frac{1}{2} \langle \delta u_{p,i} \delta u_{p,i} | H_f \rangle_p \tag{14}$$

In the frame of kinetic theory of dilute gas, pressure is linked to density and temperature by an equation of state. In the same manner, a random uncorrelated pressure (RUP) may be defined by the product of uncorrelated kinetic energy and particle number density:

$$P_p = \breve{n}_p \frac{2}{3} \delta\breve{\theta}_p \tag{15}$$

With such a definition, the velocity stress tensor may be separated into an isotropic part corresponding to the RUP and a deviatoric trace-free term $\delta\breve{\tau}_{p,ij}$,

$$\breve{n}_p \delta\breve{\sigma}_{p,ij} = -P_p \delta_{ij} + \delta\breve{\tau}_{p,ij} \tag{16}$$

Then, the momentum transport equation (10) is written,

$$\breve{n}_p \frac{\partial}{\partial t} \breve{u}_{p,i} + \breve{n}_p \breve{u}_{p,j} \frac{\partial}{\partial x_j} \breve{u}_{p,i} = -\frac{\breve{n}_p}{\tau_p} [\breve{u}_{p,i} - u_{f,i}] - \frac{\partial}{\partial x_i} P_p + \frac{\partial}{\partial x_j} \delta\breve{\tau}_{p,ij} \tag{17}$$

and, in first approximation, the deviatoric stress tensor is written in terms of the mesoscopic rate-of-strain tensor and a dynamic viscosity,

$$\delta\breve{\tau}_{p,ij} = \mu_p \left(\frac{\partial \breve{u}_{p,i}}{\partial x_j} + \frac{\partial \breve{u}_{p,j}}{\partial x_i} - \frac{2}{3} \frac{\partial \breve{u}_{p,k}}{\partial x_k} \delta_{ij} \right) \tag{18}$$

In such an approach the particle dynamic viscosity is written $\mu_p = 1/3 \breve{n}_p \tau_p \delta\breve{\theta}_p$ [6] where τ_p is the particle relaxation time. This expression can be obtained using the transport equation for the deviatoric part of the velocity variance tensor $\langle \delta u_{p,i} \delta u_{p,j} \rangle$ and supposing weak shear [10]. This closure model for the dynamic viscosity corresponds to a characteristic mixing length proportional to $\lambda_p \propto \tau_p \sqrt{2/3 \delta\breve{\theta}_p}$ which is the stopping distance due

to drag of a particle with relative velocity $\delta u_{\mathrm{p}} = \sqrt{2/3\delta\breve{\theta}_{\mathrm{p}}}$. The closure model (Eq. (18)) and the dynamic viscosity μ_{p} require the knowledge of the RUE $\delta\breve{\theta}_{\mathrm{p}}$. Modelling approaches for this quantity are developed in the next section.

2.3. Random uncorrelated kinetic energy (RUE) modelling

From the PDF equation (Eq. (2)) a general RUE transport equation can be obtained by integration from the PDF equation (2) in the same way than temperature equation in the frame of kinetic theory [5]

$$\frac{\partial}{\partial t}\breve{n}_{\mathrm{p}}\delta\breve{\theta}_{\mathrm{p}} + \frac{\partial}{\partial x_j}\breve{n}_{\mathrm{p}}\breve{u}_{\mathrm{p},j}\delta\breve{\theta}_{\mathrm{p}} = -2\frac{\breve{n}_{\mathrm{p}}}{\tau_{\mathrm{p}}}\delta\breve{\theta}_{\mathrm{p}} - (P_{\mathrm{p}}\delta_{ij} - \delta\breve{\tau}_{\mathrm{p},ij})\frac{\partial\breve{u}_{\mathrm{p},i}}{\partial x_j} - \frac{\partial}{\partial x_j}\frac{\breve{n}_{\mathrm{p}}}{2}\langle\delta u_{\mathrm{p},i}\delta u_{\mathrm{p},i}\delta u_{\mathrm{p},j}|H_{\mathrm{f}}\rangle_{\mathrm{p}} \tag{19}$$

The first rhs. term account for the RUE dissipation by drag force, the second is the compressibility effect and production due to mesoscopic velocity shear, the last term is the diffusion by RUV. In this equation, the deviatoric stress tensor $\delta\breve{\tau}_{\mathrm{p},ij}$ is modelled using the viscosity model from Eq. (18), already presented for the momentum equation (Eq. (16)). Third order RUV correlations are modelled by a diffusion term similar to the temperature Fick law which can be derived, in the frame of kinetic theory approach for particulate flows [11], from the third-order correlation transport equation as,

$$\frac{\breve{n}_{\mathrm{p}}}{2}\langle\delta u_{\mathrm{p},i}\delta u_{\mathrm{p},i}\delta u_{\mathrm{p},j}|H_{\mathrm{f}}\rangle_{\mathrm{p}} = -\kappa_{\mathrm{p}}\frac{\partial}{\partial x_j}\delta\breve{\theta}_{\mathrm{p}} \tag{20}$$

where the diffusivity coefficient is $\kappa_{\mathrm{p}} = 5/3\breve{n}_{\mathrm{p}}\tau_{\mathrm{p}}\delta\breve{\theta}_{\mathrm{p}}$.

3. Computation of Eulerian mesoscopic fields from discrete particle simulation results

In DPS approach every single k-particle follows its individual trajectory $x_{\mathrm{p},i}^{(k)}(t)$ and has its own particle velocity $u_{\mathrm{p},i}^{(k)}(t)$. Discrete particle position and velocity are given by the simple set of differential equations

$$\frac{\mathrm{d}}{\mathrm{d}t}x_{\mathrm{p},i}^{(k)} = u_{\mathrm{p},i}^{(k)}(t) \tag{21}$$

$$\frac{\mathrm{d}}{\mathrm{d}t}u_{\mathrm{p},i}^{(k)} = \frac{1}{\tau_{\mathrm{p}}}[u_{f,i}(\mathbf{x}_{\mathrm{p}}^{(k)}(t),t) - u_{\mathrm{p},i}^{(k)}(t)] \tag{22}$$

Special care has to be taken when evaluating the carrier phase velocity $\mathbf{u}_f(\mathbf{x}_{\mathrm{p}}^{(k)},t)$ at the particle location for the computation of Stokes drag law. In the present study high order interpolation methods (third-order Lagrange polynomials) are used to ensure a minimal numerical error [12].

The Eulerian model presented above is based, in theory, on an ensemble average over all particle flow realizations for a given fluid flow realization. Without inter-particle influences (directly by collisions, or through a modification of the fluid flow due to particles), an average over the Lagrangian quantities of a large number of particle is equivalent to the statistical conditional average on several particle realizations of few number of particles. In addition, interpretation of Lagrangian results in term of Eulerian mesoscopic fields such as particle number density, mesoscopic velocity or RUE requires the use of a projection procedure based on volume filtering method.

In this study, the DPS is performed with a large number of particles and field properties are obtained by projection on a regular grid with a given cell size Δx. Such projection procedure from Lagrangian to Eulerian quantities are widely used to handle the two-way coupling in DPS approach [13–16]. The salient feature of the configuration is the discontinuous distribution of the Lagrangian velocities due to the particle RUV. A control volume V_{c} around a computational node at the location $\mathbf{x}$ is defined. V_{c} should be chosen small enough with respect to the characteristic length scale of variation of the mesoscopic variables but sufficiently large to have enough particles for an accurate averaging. Mesoscopic fields such as particle number density $\bar{n}_{\mathrm{p}}$, mesoscopic velocity $\bar{\mathbf{u}}_{\mathrm{p}}$, and random uncorrelated energy $\delta\bar{\theta}_{\mathrm{p}}$ are measured in DPS as:

$$\bar{n}_{\mathrm{p}}(\mathbf{x},t) = \frac{1}{V_{\mathrm{c}}}\sum_k w(\mathbf{x}_{\mathrm{p}}^{(k)}(t) - \mathbf{x}) \tag{23}$$

$$\bar{n}_{\mathrm{p}}(\mathbf{x},t)\bar{u}_{\mathrm{p},i}(\mathbf{x},t) = \frac{1}{V_{\mathrm{c}}}\sum_k w(\mathbf{x}_{\mathrm{p}}^{(k)}(t)-\mathbf{x})u_{\mathrm{p},i}^{(k)}(t) \tag{24}$$

$$\bar{n}_{\mathrm{p}}(\mathbf{x},t)\delta\bar{\theta}_{\mathrm{p}}(\mathbf{x},t) = \frac{1}{2}\frac{1}{V_{\mathrm{c}}}\sum_k w(\mathbf{x}_{\mathrm{p}}^{(k)}(t)-\mathbf{x})[u_{\mathrm{p},i}^{(k)}(t)]^2 - \frac{1}{2}\bar{n}_{\mathrm{p}}(\mathbf{x},t)\bar{u}_{\mathrm{p},i}^2(\mathbf{x},t) \tag{25}$$

where $w(\mathbf{x}_{\mathrm{p}}^{(k)}(t)-\mathbf{x})$ is a weight function. Definitions of several different projections are presented in Table 1. The top-hat and volumic (based on Schoenberg M_2 spline) projectors are written for two different widths, a Gaussian projector is also presented. We restrict our attention to second-order space accurate projectors for two reasons. Firstly, higher order projector weight function should have negative loops leading to unphysical negative particle number density values when very few particles are present. Secondly, the corresponding convergence rate in terms of the particle number is slower [16]. Integral of the different projector kernels over the control volume is unity to ensure the globally (ie. for infinite particle number) quantity mean conservation by projection. It must be noticed that the box, large box, and large volumic projector are also locally mean-conservative for finite particle number densities [14]. The characteristic length scale of the projector is evaluated by doubling the standard deviation of the weight function σ:

$$\sigma^2 = \frac{1}{V_{\mathrm{c}}}\int_{V_{\mathrm{c}}} |\mathbf{x}_{\mathrm{p}}-\mathbf{x}|^2 w(\mathbf{x}_{\mathrm{p}}-\mathbf{x})\,\mathrm{d}x_{\mathrm{p},1}\,\mathrm{d}x_{\mathrm{p},2}\,\mathrm{d}x_{\mathrm{p},3} \tag{26}$$

Leading to the characteristic length scale classification of the retained projectors:

$$\text{Large box} > \text{Large volumic} > \text{Box} \approx \text{Gaussian} > \text{Volumic} \tag{27}$$

3.1. Validation on 1D synthetic case

Tests of these projection procedures were performed on one-dimensional synthetic case. The box, volumic, and Gaussian 1D projection kernels are presented in Fig. 2. N_{p} particles are randomly distributed on a one-dimensional grid with an equidistant node spacing Δx of N nodes. The mean particle number per cell is $N_{\mathrm{p}}/N = \langle n_{\mathrm{p}}\rangle\Delta x$ in 1D. The particle distribution is projected on the grid (Eq. (23)) to obtain the mesoscopic particle number density. The conservation of mean quantities by Gaussian and volumic projection is evaluated for the mean projected number density $\langle\bar{n}_{\mathrm{p}}\rangle$ (Fig. 3). As expected the associated error is decreasing when the mean particle number per cell is increasing. It can easily be shown that this bias is avoided in the case of equally spaced particles and is due to non homogeneous particle repartition in every projection grid cell.

We focus now our attention on kinetic quantities. A turbulent-like velocity field ($\breve{u}_{\mathrm{p}}$) and a Gaussian uncorrelated white noise ($\delta u_{\mathrm{p}}^{(k)}$) are given to the randomly placed particles:

$$u_{\mathrm{p}}^{(k)} = \breve{u}_{\mathrm{p}}(x_{\mathrm{p}}^{(k)}) + \delta u_{\mathrm{p}}^{(k)} \tag{28}$$

The velocity field follows a Passot–Pouquet type spectrum defined on 32 modes (presented in the study), but tests using a $-5/3$ decrease rate spectrum show similar results. The energy of the noise has been chosen to be 30% of the mesoscopic energy, which correspond to the maximum of the particle random uncorrelated energy

Table 1
Projection procedure definitions in 3D

Projection	Control volume V_{c}	Weight function $w(\mathbf{x}_{\mathrm{p}}^{(k)}-\mathbf{x})$	Characteristic length 2σ
Box	$(\Delta x)^3$	1	Δx
Large box	$(2\Delta x)^3$	1	$2\Delta x$
Volumic	$(\Delta x)^3$	$\prod_{i=1}^3\left(2-2\frac{\lvert x_{\mathrm{p},i}^{(k)}-x_i\rvert}{\Delta x/2}\right)$	$\frac{\Delta x}{\sqrt{2}}$
Large volumic	$(2\Delta x)^3$	$\frac{1}{2^3}\prod_{i=1}^3\left(1-\frac{\lvert x_{\mathrm{p},i}^{(k)}-x_i\rvert}{\Delta x}\right)$	$\sqrt{2}\Delta x$
Gaussian	$(2\Delta x)^3$	$\frac{(2\Delta x)^3}{\mathrm{erf}(\sqrt{6})^3}\left(\frac{6}{\pi\Delta x^2}\right)^{\frac{3}{2}}\exp\left(-\frac{6\lvert\mathbf{x}_{\mathrm{p}}^{(k)}-\mathbf{x}\rvert^2}{\Delta x^2}\right)$	$\left(1-\frac{2\sqrt{6}\mathrm{e}^{-6}}{\sqrt{\pi}\mathrm{erf}(\sqrt{6})}\right)\Delta x \approx \Delta x$

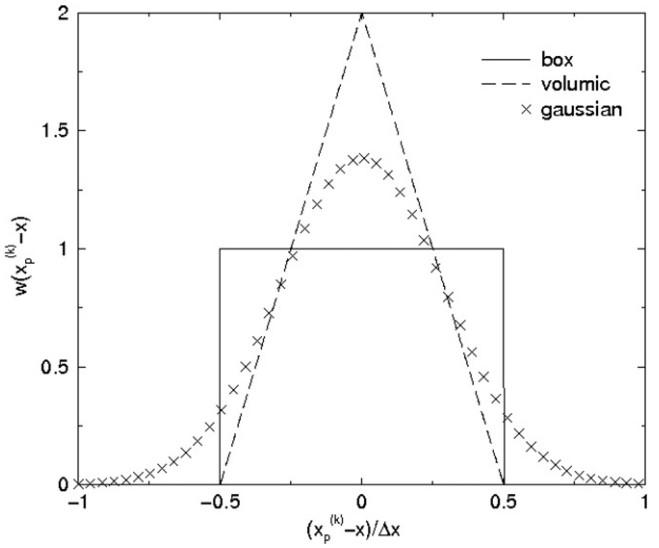

Fig. 2. Weight function of the different projection in 1D.

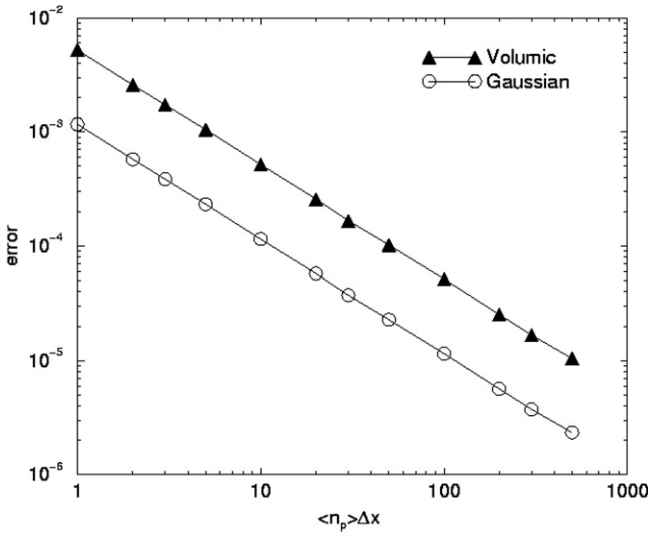

Fig. 3. Evolution of the conservation of the projected particle number with the mean particle number per cell (error $= (\langle \bar{n}_p \rangle - \langle n_p \rangle)^2 / \langle n_p \rangle^2$) for the 1D synthetic case.

measured by Février et al. [1] in stationary homogeneous isotropic turbulence. Particle properties are then projected on a one-dimensional 64 node grid of length 2π. Substituting Eq. (28) in Eq. (24) leads to:

$$\bar{n}_p \bar{u}_p = \frac{1}{V_c} \sum_k w(u_p^{(k)} - x) \breve{u}_p(x_p^{(k)}) + \frac{1}{V_c} \sum_k w(x_p^{(k)} - x) \delta u_p^{(k)} \tag{29}$$

$$\bar{n}_p \bar{u}_p = \bar{n}_p \overline{\breve{u}_p} + \bar{n}_p \overline{\delta v} \tag{30}$$

To identify the projected velocity $\bar{u}_p$ to the mesoscopic velocity $\breve{u}_p$, the projection procedure must be able to eliminate the noise $\overline{\delta u_p}$ and must not affect the mesoscopic velocity field. The difference between the projected velocity fields and the non projected mesoscopic velocity distribution is evaluated by the quadratic error:

$$\mathrm{Error}(\phi) = \frac{\langle (\phi(x) - \breve{u}_{\mathrm{p}}(x))^2 \rangle}{\langle \breve{u}_{\mathrm{p}}(x)^2 \rangle} \tag{31}$$

where ϕ is the field to be tested, ie. projected velocity with added noise $\overline{u_{\mathrm{p}}}$ or without noise $\overline{\breve{u}_{\mathrm{p}}}$. The same Lagrangian field is projected with the different projections. To obtain statistical convergence, average is performed on 5000 different realizations of the velocity field. This procedure is repeated for several values of the particle number per cell of the projection grid, from one to thousand. Fig. 4 shows the dependence of the velocity projection error (computed from Eq. (31) with $\phi = \overline{\breve{u}_{\mathrm{p}}}$) on the particle number per cell for the different projection procedures. The error decreases when increasing the particle number, but a systematic error occurs even for a large particle number density. For more than 10 particles per cell, the related error arises in decreasing order from the large box projector, the large volumetric filter, the box filter, and the volumetric filter. In the noisy case (Fig. 5), i.e. $\phi = \overline{u_{\mathrm{p}}}$ in Eq. (31), more than 100 particles per cell are needed to reach the system-

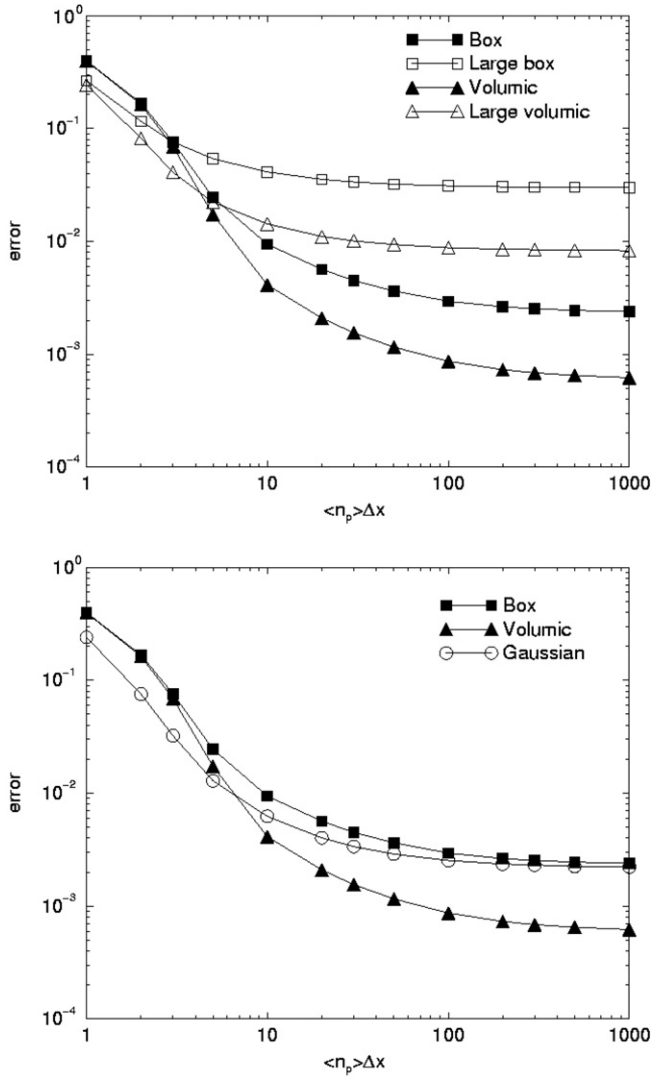

Fig. 4. Dependence of velocity quadratic error (given by Eq. (31)) due to the projection procedure on the particle number per cell for 1D synthetic case. Particle velocity distribution is given from the interpolation of a continuous turbulent field on the particle position. Upper figure: comparison between box, large box, volumic, and large volumic projections. Lower figure: comparison between box, volumic, and Gaussian projections at the bottom.

atic projector error level, but the projector efficiency classification remains the same. In addition to the statistical error due to the finite number of particles in the averaging cell, Boivin et al. [14] showed that such projection procedures are equivalent to a filtering of the length scales smaller than the control volume size which limit high gradient values. This spatial error can be limited by using smaller control volume, but this increases however the statistical error due to particle number. A different alternative would be to use a projection kernel with a smaller characteristic length scale. It can be noticed that volumic-type projectors returns better results than box-type projectors. A compromise between small systematic error and accuracy for small particle number density is to use the Gaussian projector on a large control volume (see Table 1) but having the box projection characteristic length scale. The Gaussian projector error is comparable to the box projection error for high particle numbers and to the large box for small particle number.

To analyse more in details the projection error, the energy spectra of $\breve{u}_p$, $\overline{\breve{u}_p}$, $\overline{\delta u_p}$, and $\bar{u}_p$ are presented in Figs. 6–8 with the Gaussian projector for 2, 20, and 200 mean particle number per cell of the projection grid. For all the cases the projected mesoscopic velocity energy (Fig. 6) spectra follow the one of the mesoscopic velocity at large scales. The projected mesoscopic velocity ($\overline{\breve{u}_p}$) energy spectra for the 200 mean particle num-

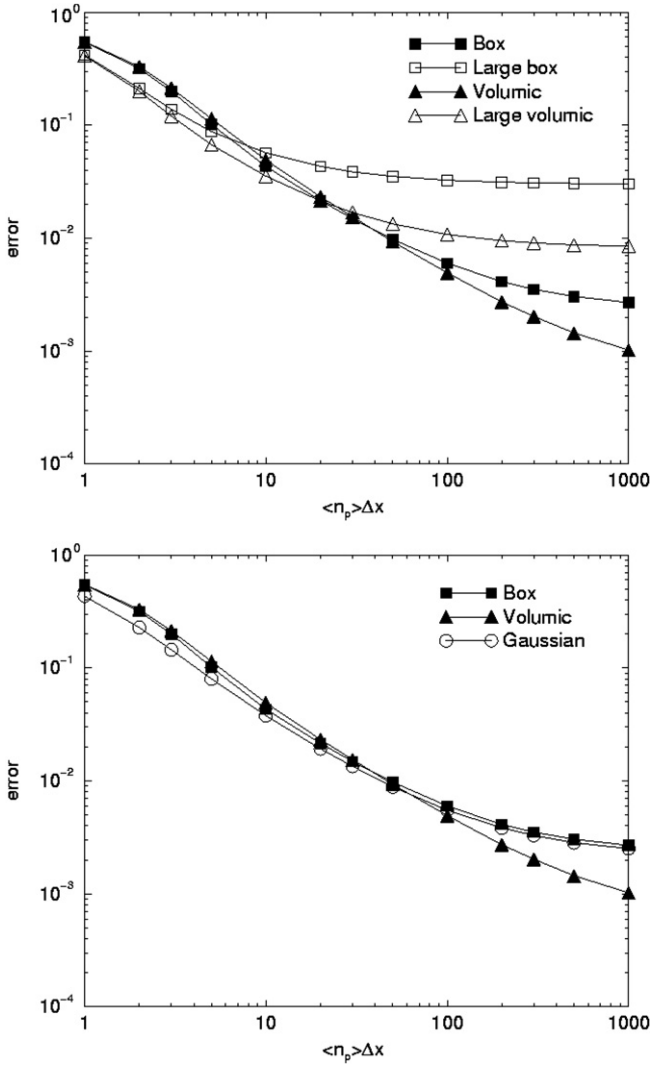

Fig. 5. Same caption as Fig. 4. Particle velocity is the velocity of the continuous field at their location with an added Gaussian white noise of 30% energy.

ber per cell case underestimates the energy at small scales comparing to the $\breve{u}_p$ energy spectra. This behaviour is the mark of the spatial error detailed before. In the case of two particles per cell case, the spectrum presents an unphysical overestimation of the small scale energy. This effect is avoided by increasing the mean particle number density, n_p so that the spectra for 20 and 200 particles per cell are nearly identical for all waves numbers. For equally spaced particles, the error is removed, even for the case with the lowest particle number per cell (not presented here) proving that the overestimation of the velocity spectrum induced by the projection procedure is due to the random repartition of the particles.

Fig. 7 shows the energy spectra of the projected noise ($\overline{\delta u_p}$). These spectra are mainly flat and their average energy level decreases quasi-linearly when the particle number density increases. The noise spectra energy levels are comparable with the correlated energy ones. More precisely, this level can be evaluated. The energy

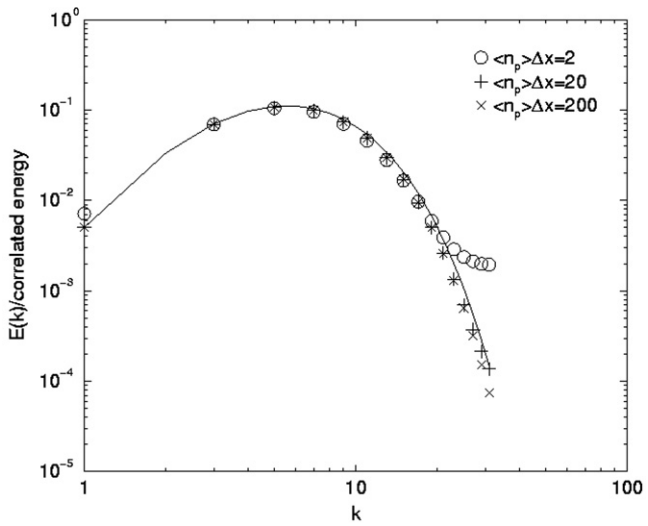

Fig. 6. Dependence of the projected mesoscopic energy spectra using the Gaussian projector on the mean number of particles per cell. 1D synthetic case. The line is the mesoscopic energy spectra.

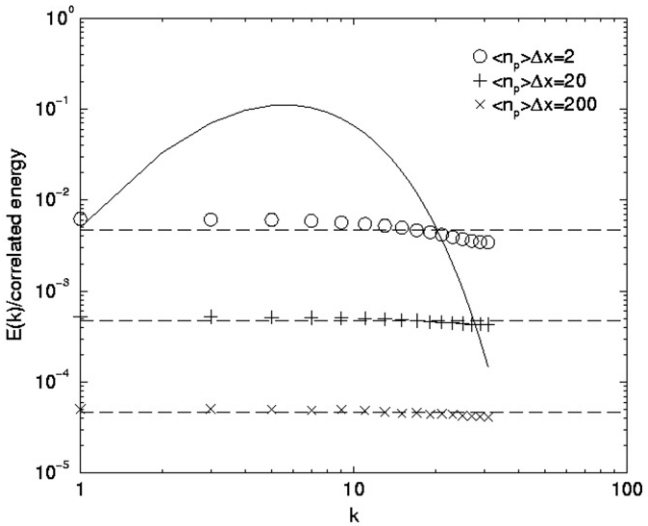

Fig. 7. Dependence of the projected noise energy spectra using the Gaussian projector on the mean number of particles per cell. 1D synthetic case. The continuous line is the mesoscopic energy spectra. The horizontal dashed lines correspond to the noise spectrum models (Eq. (33)).

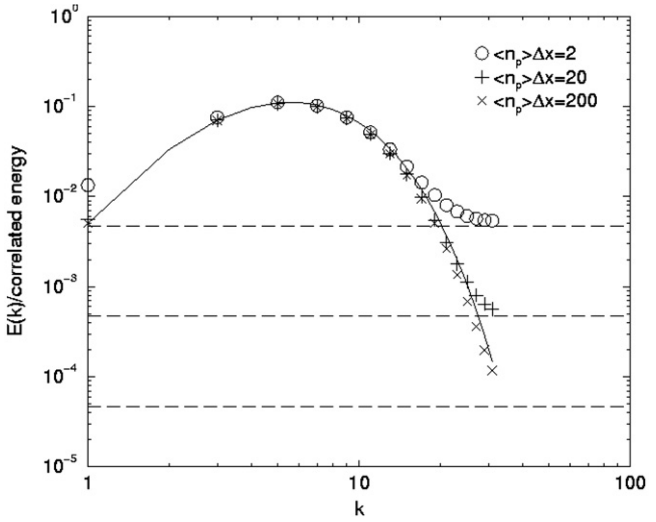

Fig. 8. Dependence of the projected mesoscopic energy spectra with added noise using the Gaussian projector on the mean number of particles per cell. 1D synthetic case. The continuous line is the mesoscopic energy spectra. The horizontal dashed lines correspond to the noise spectrum models (Eq. (33)).

spectrum of a discrete white noise on N_p equally spaced particles is constant up to the Nyquist frequency ($N_p/2 = \langle n_p \rangle N\Delta x/2$). Considering that the spectrum integral gives the random uncorrelated energy, the energy spectrum of the discrete noise is

$$E_{\delta u_p}(k) = \frac{N\Delta x}{2\pi}\left(\frac{N_p}{2} - 1\right)^{-1} \delta q_p^2 \tag{32}$$

$$E_{\delta u_p}(k) \approx \frac{1}{\pi \langle n_p \rangle} \delta q_p^2 \tag{33}$$

For non-homogeneous particle distribution, Eq. (33) can be used as a noise spectrum level estimation. Comparing the projected noise spectra level with the non projected noise model level, the particle density effect is recovered and the mean level too (about 2% error). The projection procedure is just filtering the noise and cut off all the components with wave numbers larger than $N/2$.

We now consider the projection of mesoscopic velocity with added noise (Fig. 8). At small scales the energy spectrum of $\overline{\tilde{u}_p}$ obtained with 2 or 20 mean particle number per cell follows the one of the noise. A statistical error occurs and the projection is not able to eliminate noise of the discrete velocity field. By increasing the number of particle the energy of the projected noise becomes negligible against the mesoscopic energy at all length scales. An a-posteriori validity criteria in the computation of the mesoscopic energy spectra with added noise is introduced:

$$E_{\tilde{u}_p}(k) > \frac{1}{\pi \langle n_p \rangle} \delta q_p^2 \quad \text{for all } k \tag{34}$$

To resume, when obtaining continuous Eulerian fields from discrete Lagrangian quantities by projection, errors are mainly due to a statistical error and to an intrinsic filtering (or spatial error) at small scales. By using a well chosen projector (e.g. Gaussian projection) with enough of particles (more than 10 particles per cell), it is possible to circumvent the problem in a satisfactory manner.

3.2. Validation from DPS results

Finally to validate the Gaussian projection, two DPS have been performed with 10 and 80 millions Lagrangian particles. Particles are randomly placed in the computational domain of length 2π with the fluid velocity at their position. Initial Lagrangian quantities are then projected with a Gaussian filter on a 64^3 and

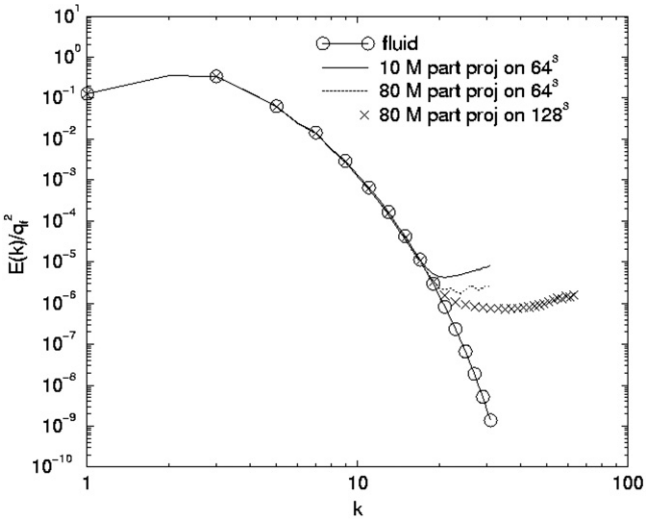

Fig. 9. Comparison of mesoscopic energy spectra measured from DPS results at the initialisation with $\mathbf{u}_p^{(k)}(t=0) = \mathbf{u}_f(\mathbf{x}_p^{(k)}(t=0),(t=0))$. DPS with 10^7 or 8×10^7 particles projected on a 64^3 or 128^3 grid with the Gaussian projector.

128^3 node grids. For the coarser case, 10 millions of particles projected on a 64^3 grid cell (approximately 38 particles by cell) with a Δx equal to the computing mesh size, the projected spectrum is identical to the fluid one for k smaller than 18 (Fig. 9). For larger value of k, the energy spectrum of the projected velocity shows an unphysical increase but remains 10^4 smaller than the effective values measured in the energetic region. As expected, Fig. 9 shows that this effect can be diminished by increasing the particle number and decreasing the projection cell size but leading to very expansive simulation costs.

The 10 and 80 million DPS are performed. Instantaneous Lagrangian results, corresponding to a case with large RUE intensity (≈16% of the mesoscopic energy is measured) and particle segregation effects, are analysed. The energy spectra of mesoscopic velocities obtained by projection on a 64^3 (Fig. 10) are nearly identical for the two DPS results, no statistical bias is observed so that 10 million particles is sufficient to analyse mes-

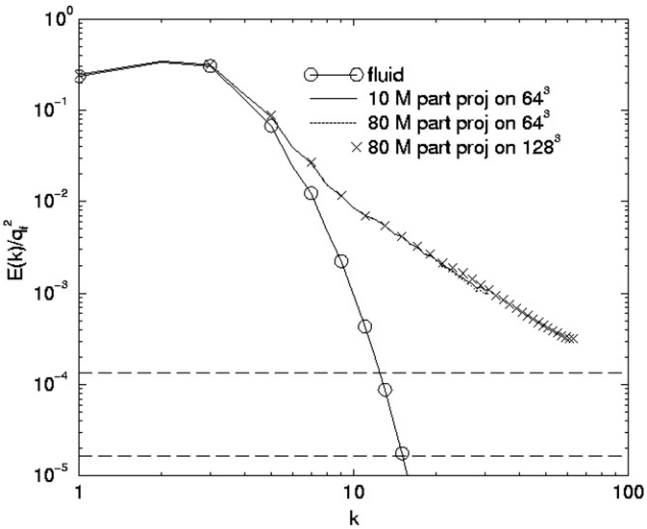

Fig. 10. Comparison of mesoscopic energy spectra measured from DPS results. DPS with 10^7 or 8×10^7 particles projected on a 64^3 or 128^3 grid with the Gaussian projector. Case $St = 0.53$ at time $t = 10.8$. Horizontal dashed lines are the lower limit of spectrum validity given by Eq. (35) (upper line is for cases 10^7 particles projected on 64^3 and 8×10^7 particles projected on 128^3 grid; lower line is for case 8×10^7 particles projected on 64^3 grid).

oscopic velocity fields in term of energy spectra. Indeed, these spectra follow the one obtained by projection on a finer grid (128^3) up to the higher wave number (Fig. 10). The one-dimensional noise spectrum model (Eq. (33)) is extended for the three-dimensional spectrum by replacing the total number of particle by the number of particles in only one direction ($\langle n_p \rangle \Delta x^3 N$):

$$E_{\vec{u}_p}(k) > \frac{1}{\pi \langle n_p \rangle \Delta x^2} \delta q_p^2 \quad \text{for all } k \tag{35}$$

We notice in Fig. 10 that the mesoscopic energy spectrum validity criterion (Eq. (35)) is satisfied. This criterion is of course questionable because particle distribution is far from homogeneity and RUE is not uniform, but it could be considered as a spectrum validity indicator. The Gaussian projector is really able to limit the intrinsic error of the projection procedure and is used to obtain mesoscopic fields from DPS results with 10 million particles for 64^3 projection cells in the rest of the paper.

4. Homogeneous isotropic decaying turbulence test case

Homogeneous isotropic turbulence is one of the classical cases where dynamics and dispersion of particle laden flows can be studied. This has been done extensively using the DPS approach coupled with fluid turbulence DNS and many results leading to improve the detailed understanding of the mechanisms occurring in particle laden turbulent flows were obtained by such methods. Comparison of DPS + DNS results in decreasing homogeneous isotropic turbulence [17] with experimental measurements of particle dispersion in grid generated turbulence [18] shows that essential features of the particle dynamics can be captured. In addition, such approach allows to analyse the preferential concentration effect which occurs for particles with relaxation time of the same order than the Kolmogorov time scale.

Therefore, for the sake of simplicity, the case of decaying homogeneous isotropic turbulence is studied here to investigate the accuracy of the mesocopic Eulerian approach in predicting the particulate flows. The carrier phase is initially supposed to have uniform density, the velocity field to be divergence free, and the kinetic energy to follow a Passot–Pouquet spectrum [19]. After roughly one turn over time of the energy containing eddies, the velocity field is supposed to represent a realistic turbulent flow and the dispersed phase is coupled with the fluid flow. At the particle injection time, the Reynolds number based on the integral length scale measured from the longitudinal velocity autocorrelation function is $Re_L = 13.6$. For DPS initial conditions, particles are randomly and homogeneously distributed in space and the initial particle velocities are given equal to the carrier phase velocity at the particle location. For the mesoscopic Eulerian computations, the same conditions correspond to a uniform particle number density field and a mesocopic particle velocity field identical to the carrier phase velocity field. The uncorrelated kinetic energy (RUE) field is initialized with a very small uniform value (less than 0.02% of the mean particle kinetic energy) and is developing very quickly during the simulation showing a weak influence of the given initial value. The spatial resolution of the gaseous phase computation in the DPS + DNS approach is 64^3 and a total of 10 million individual particles are tracked in the computational domain.

4.1. Numerical methods

The mesoscopic Eulerian simulation is performed using a different code (AVBP [20]) then the DPS reference solution (NTMIX [15]). AVBP offers several spatial and temporal schemes. In the present study a central second-order spatial scheme with a second order temporal correction (Lax Wendroff) was used. Comparison to third order Runge–Kutta time stepping showed no significant improvement of the numerical accuracy. NTMIX uses a sixth-order spectral like scheme [21] on cartesian grids, third-order Runge–Kutta time stepping, and third-order Lagrange polynomial interpolation. The time step is limited in both tools by a CFL for the carrier phase. A second CFL number based on the Eulerian cell size and the maximum particle velocity is used for time step limitation in the DPS.The CFL criteria are fixed to 0.5 in both codes. In the Eulerian simulation and in the Lagrangian simulation the dispersed phase is advanced with the same time step as the carrier phase. For the investigated Stokes numbers the characteristic time scale of the particles τ_p is of one order of magnitude larger than the numerical time step. Both numerical tools use domain decomposition

and MPI for parallel computation. For the test cases carrier phase solutions are initially identical and velocity spectra superpose.

The carrier phase kinetic energy of the two codes are identical (Fig. 11). Furthermore, the kinetic energy spectra at a non dimensional time of 10.8 are very similar until the Kolmogorov wave number $(1/\eta_K)$ which is 7.7 in non-dimensional units (see Fig. 12).

In the mesoscopic Eulerian simulation, the dispersed phase is computed using the same numerical method as the carrier phase, imposing an additional limit on the time step due to particle relaxation time ($\tau_p \gg \Delta t$).

Comparisons between Eulerian an Lagrangian simulation results are performed considering several particle variables. First, Lagrangian statistical properties of the dispersed phase such as particle kinetic energy and particle-fluid velocity correlation are investigated. Second, local instantaneous mesoscopic Eulerian fields such as particle number density $\breve{n}_p$, mesoscopic velocity $\breve{u}_{p,i}$, and random uncorrelated kinetic energy $\delta\breve{\theta}_p$ fields measured from both the Lagrangian and Eulerian simulations are compared. Finally, the mesoscopic particle kinetic energy spectra $E_p(k)$ computed from both Lagrangian and Eulerian simulation results are compared.

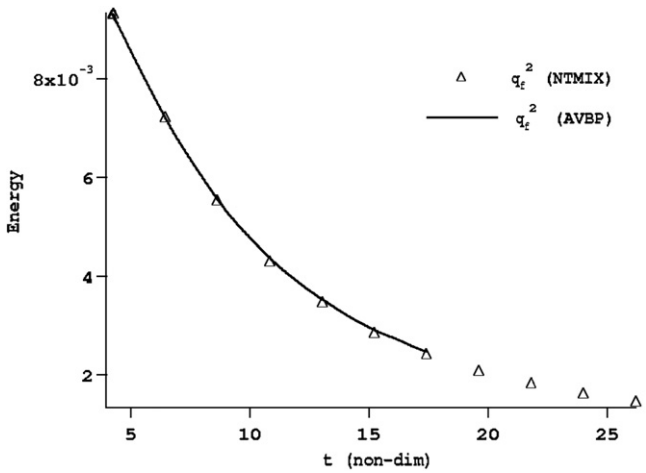

Fig. 11. Comparison of the mean carrier phase turbulent kinetic energy q_f^2 computed from AVBP simulations (line) using a second-order difference scheme with the one computed from NTMIX simulations (triangles) using a spectral like scheme [21].

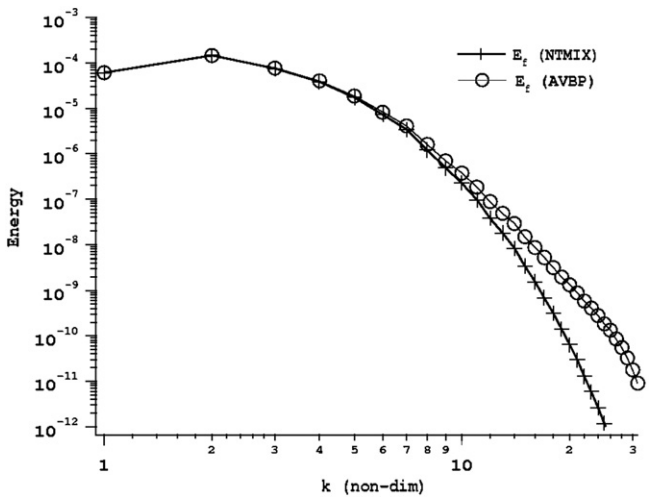

Fig. 12. Kinetic energy spectra of the carrier phase from simulations with the two numerical codes used in this study at time $t = 10.8$.

4.2. Spatial averaged quantities over the whole computational domain

Mean particle kinetic energy q_p^2 and fluid-particle correlation q_{fp} derived by spatial averaging $\{\cdot\}$ should be identical in the two simulations and therefore constitute a first step of comparison. In the present test case of decreasing homogeneous isotropic turbulence those quantities vary in time. The mean properties are computed by averaging over the computational domain and may be written from the Eulerian simulation results as

$$q_f^2 = \frac{1}{2}\{u_{f,i}u_{f,i}\} \tag{36}$$

$$q_{fp} = \{u_{f,i}\breve{u}_{p,i}\}_p \tag{37}$$

$$\breve{q}_p^2 = \frac{1}{2}\{\breve{u}_{p,i}\breve{u}_{p,i}\}_p \tag{38}$$

and from the DPS ones,

$$q_{fp} = \frac{1}{N}\sum_k u_{p,i}^{(k)} u_{f,i}(\mathbf{x}_p^{(k)}) \tag{39}$$

$$q_p^2 = \frac{1}{N}\sum_k \frac{1}{2} u_{p,i}^{(k)} u_{p,i}^{(k)} \tag{40}$$

The spatial averaged uncorrelated kinetic energy (RUE) computed from DPS results is given by

$$\delta q_p^2 = \{\delta\breve{\theta}_p\}_p \tag{41}$$

with the local RUE $\delta\breve{\theta}_p$ given by Eq. (25).

4.3. Kinetic energy spectra

Using the Fourier transformed velocities of the carrier phase $\hat{u}_{f,i}(k) = \mathcal{F}(u_{f,i}(x))$ and dispersed phase $\hat{u}_{p,i}(k) = \mathcal{F}(\breve{u}_{p,i}(x))$ one can construct three-dimensional fluid and particle energy spectra

$$E_f(k) = \frac{1}{2}\hat{u}_{f,i}(k)\hat{u}_{f,i}(k) \tag{42}$$

$$E_p(k) = \frac{1}{2}\hat{u}_{p,i}(k)\hat{u}_{p,i}(k) \tag{43}$$

For given turbulent flow the undisturbed carrier phase kinetic energy follows the standard Kolmogorov spectrum. Here the interest lies on the behaviour of the spectra of the mesoscopic particle kinetic energy. In particular, whereas the carrier phase is considered incompressible, segregation effects measured in DPS show that there must be a compressible part in the mesoscopic dispersed phase velocity spectrum. Following Kraichnan [22], the compressible effect on the mesoscopic particle kinetic energy spectrum can be characterized by dividing the spectral velocity into a compressible and an incompressible (solenoidal) component

$$\hat{u}_{p,i}^c = \frac{\kappa_i\kappa_j}{\kappa^2}\hat{u}_{p,j} \tag{44}$$

$$\hat{u}_{p,i}^s = \left(1 - \frac{\kappa_i\kappa_j}{\kappa^2}\right)\hat{u}_{p,j} \tag{45}$$

This orthogonal decomposition allows to construct a compressible and a solenoidal energy spectra such that the sum equals to the total energy spectrum

$$E_p^c(k) = \frac{1}{2}\hat{u}_{p,i}^c(k)\hat{u}_{p,i}^c(k) \tag{46}$$

$$E_p^s(k) = \frac{1}{2}\hat{u}_{p,i}^s(k)\hat{u}_{p,i}^s(k) \tag{47}$$

5. Simulations results and discussion

Preliminary computations with a simplified Eulerian formalism, neglecting the RUV kinetic stress terms, gave encouraging results for the same test case [23]. In the case of tracer particles (small Stokes number limit), the RUV contribution tends towards zero with respect to the full particle velocity [1] and such simplified Eulerian approach is expected to accurately describe the particle dynamics [2,3]. Moreover, a crucial assumption of such modelling approach, the particle velocity uniqueness, is not verified for particle Stokes number based on Kolmogorov time scale greater than unity. Therefore, the Eulerian approach for the dispersed phase must account specifically for the effects of crossing between the particle trajectories. In particular, this crossing mechanism is expected to reduce the particle segregation effect induces by the interaction with the turbulent eddies when the particle inertia is increasing. Such a mechanism is accounted for in the mesoscopic Eulerian approach through the pressure-like term in the momentum equation due to the second-order RUV moments. As pointed out in Section 4, Eulerian methods should be well suited to describe the particle dynamics [2] for particle relaxation times small compared to the Kolmogorov time scale. It is therefore interesting to study how the Eulerian description behaves outside this range. Therefore in a first step the results of DPS and the Eulerian model are compared for the Stokes number of $St_K = 0.17$. In a second step an heuristic extension of the proposed model overcoming the numerical difficulties encountered due to massive segregation is presented and results are compared for a Stokes number based on the macroscopic dissipative time scale of $St = 0.53$ according to a Stokes number value, based on the Kolmogorov time scale, $St_K = 2.2$. Despite the small maximum particulate mean Reynolds number reached in Lagrangian simulation (always $<5 \times 10^{-2}$), local instantaneous particulate Reynolds number can be large when occasionally particles cross vortices and are given high speed. Anyways, the drag force assumption is done provided that the DPS and the Mesoscopic Eulerian simulations are computed under the same assumptions. Eulerian results presented here are obtained with the RUE transport equation (Eq. (19)).

5.1. Comparison at $St_K = 0.17$

At Stokes numbers as small as $St = 0.042$ based on the dissipative time scale $\tau^+ (= q_f^2/\varepsilon)$ the particles are expected to follow closely the carrier phase velocity and the uncorrelated velocity contribution to the particle dynamics is very small. In Fig. 13 the integral quantities of mesoscopic particle kinetic energy $\breve{q}_p^2$, fluid-particle

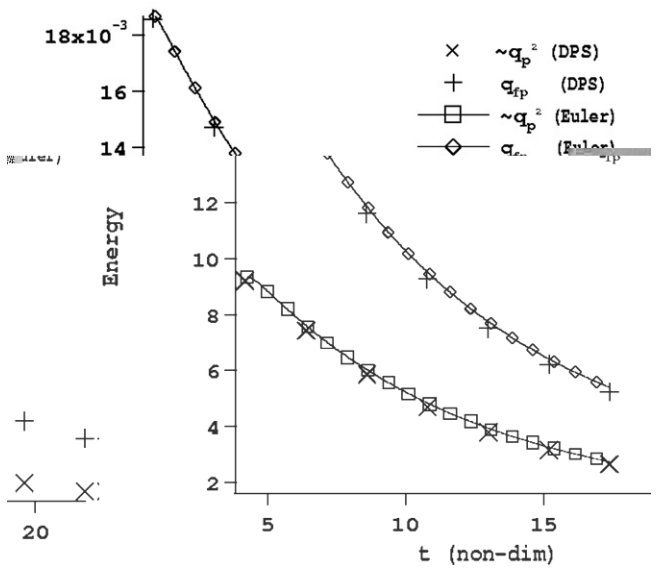

Fig. 13. Comparison of mean mesoscopic particle kinetic energy and fluid-particle velocity correlation from DPS and Eulerian simulation for the test case of $St_K = 0.17$.

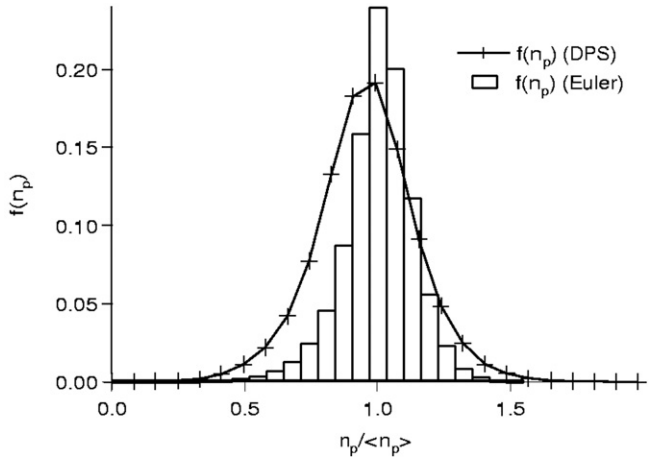

Fig. 14. Comparison of particle number density PDF measured from Lagrangian simulation with the one from mesoscopic Eulerian simulation. Case $St_K = 0.17$ at $t = 10.8$.

correlation q_{fp} of the Eulerian simulation are compared to the DPS results. Temporal evolution of particle kinetic energy and fluid-particle correlation are well predicted by the Eulerian simulation.

RUE measured in DPS ($\approx 10^{-2} q_p^2$) is of the same order of numerical error. Then the predicted RUE is of two orders of magnitude lower than the mesoscopic kinetic energy, the contribution of RUE can be neglected in this case.

Fig. 14 shows the probability to find a computational cell with a given value for the number density in the Eulerian prediction and the DPS reference result at $t = 10.8$. The distribution of the Eulerian number density is less wide than the DPS distribution. If the mesoscopic velocity is well predicted in the Eulerian simulation, a possible cause of the non-matching number density distributions may be the numerical scheme dispersion leading to a more homogeneous particle number density.

As an instantaneous local quantity the normalized particle number density is shown in Fig. 15 for the x–y plane crossing the computational domain center at the simulation time $t = 10.8$. This corresponds to roughly 18 particle relaxation times (τ_p) and two dissipative times scales (τ^+) of the carrier phase. It shows that the Eulerian number density prediction is quantitatively close to the DPS result. Regions with high and low particle number densities are well correlated in the two approaches.

Fig. 16 shows the total mesoscopic particle kinetic energy spectra and the compressible kinetic energy spectra computed from Lagrangian and Eulerian simulation results. The mesoscopic particle kinetic energy spectrum follows closely the spectrum of the carrier phase at large scales. Up to the *kink* in the DPS energy spectra, the spectra computed from the Eulerian Simulation match well those from the DPS. As shown in Section 3, this *kink* is probably unphysical and is due to a numerical error induced by the non-homogeneous particle distribution.

In case of small Stokes number, the mesoscopic simulation is able to predict integral quantities such as particle energy and also local quantities such as segregation. Results with Eulerian mesoscopic approach are very similar to the ones obtained using the Eulerian equilibrium approach propose by Rani and Balachandar [3,24].

5.2. Comparison at $St_K = 2.2$

Preliminary tests with Stokes numbers of $St_K = 2.2$ failed since large segregation effects imply very stiff local gradients in the number density distribution (shock like) that caused dispersion errors in the numerical scheme [25]. Tests with increased Eulerian simulation grid resolution up to 256^3 was unsuccessful. Supposing that the numerical resolution of the model is insufficient, several possibilities exist to circumvent this difficulty: a different numerical scheme using up-winding or flux limiters are clearly able to capture those strong gradients but imply some type of numerical diffusion. For the computation of the number density in the equilibrium Eulerian approach with a limited Stokes number range Rani and Balachandar [3,24] use a spectral viscosity to

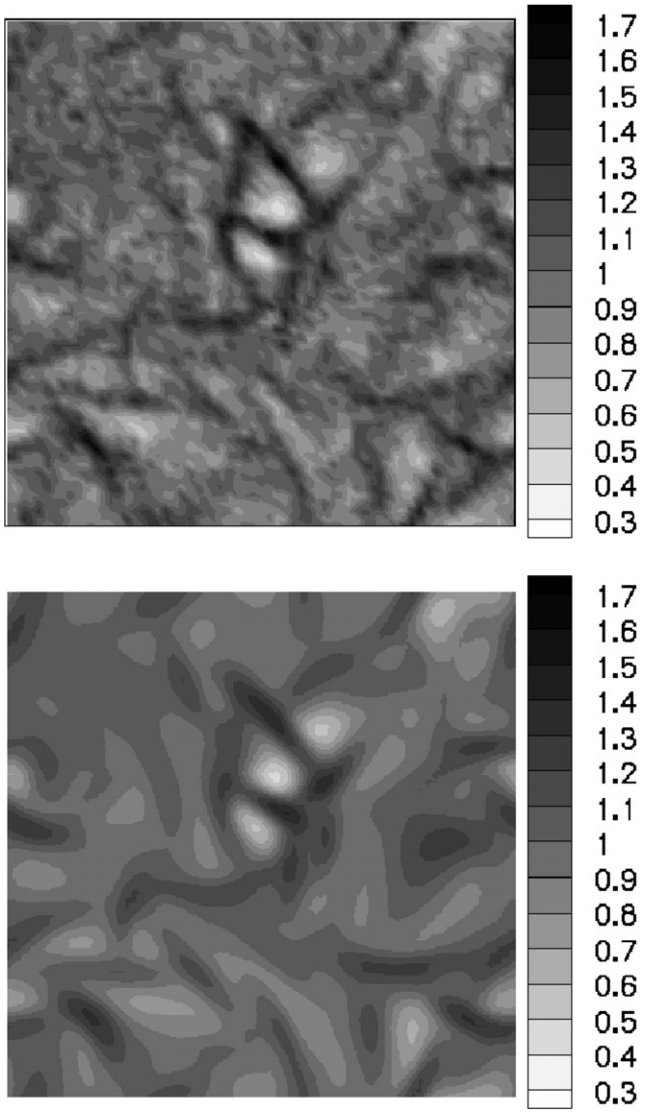

Fig. 15. Comparison of the normalized particle number density $\breve{n}/\langle\breve{n}\rangle$ measured from the Lagrangian simulation (upper graph, resolution 64^3) with the one given by the Eulerian simulation (lower graph, resolution 64^3) at the non-dimensional time $t = 10.8$, case $St_K = 0.17$. The drawing plane is parallel to the x–y reference plane and crosses the computational domain center.

overcome this difficulty. Increasing spatial resolution increases strongly numerical cost. The origin of the preferential concentration is due to the compressibility of the particle number density field. A pure diffusivity added to the evolution of the number density field would bias the conservative transport of the particle velocity. The origin of the compressibility is the compressible component of the mesoscopic particle velocity field.

At this point it was found preferable to act on the compressible component of the mesoscopic velocity field to circumvent the measured difficulties associated with steep gradients. This leads to compute for a modified mesoscopic velocity $\breve{\tilde{u}}_{\mathrm{p},i}$ transport equation and consequently a modified particle number density field $\bar{\breve{n}}_{\mathrm{p}}$. The compressible component of the mesoscopic velocity is modified by introducing a subgrid bulk viscosity ξ_{sgs}

$$\frac{\partial}{\partial t}\bar{\breve{n}}_{\mathrm{p}}\breve{\tilde{u}}_{\mathrm{p},i}+\frac{\partial}{\partial x_j}\bar{\breve{n}}_{\mathrm{p}}\breve{\tilde{u}}_{\mathrm{p},i}\breve{\tilde{u}}_{\mathrm{p},j}=-\frac{\partial}{\partial x_i}\bar{P}_{QB}+\frac{\partial}{\partial x_j}\bar{\tau}_{ij}-\frac{\bar{\bar{n}}_{\mathrm{p}}}{\tau_{\mathrm{p}}}(\breve{\tilde{u}}_{\mathrm{p},i}-\tilde{u}_{\mathrm{f},i})+\frac{\partial}{\partial x_i}\left(\xi_{\mathrm{sgs}}\frac{\partial}{\partial x_k}\breve{\tilde{u}}_{\mathrm{p},k}\right) \tag{48}$$

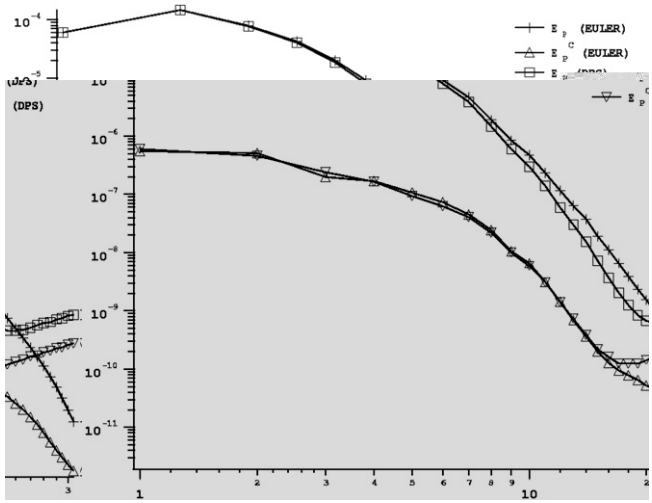

Fig. 16. Comparison of total and compressible particle mesoscopic kinetic energy spectra computed from DPS and Eulerian simulation results for the test case with $St_K = 0.17$ at t=10.8.

The subgrid model has the form of a bulk viscous term $\xi_{sgs}\partial\tilde{\breve{u}}_k/\partial x_k\delta_{ij}$ which is added to the shear viscosity term $\delta\breve{\tau}_{p,ij}$ in Eq. (18). The subgrid bulk viscosity is mesh size dependent: $(\xi_{sgs} = C_\xi\bar{\breve{n}}_p(\Delta x)^2|\partial\tilde{\breve{u}}_k/\partial x_k|)$. The parameter C_ξ in the bulk viscosity expression is fixed equal to 50 which is the smallest value allowing to run the case with $St_K = 2.2$. The RUE transport equation (Eq. (19)) is not modified.

In homogeneous turbulence, the spatial average of this bulk viscous term is zero, still it acts locally and leads to a more homogeneous number density field. Simulations have been carried out for several particle relaxation times. The following computation with a Stokes number of $St_K = 2.2$ is performed with this heuristically introduced bulk viscosity and compared to the DPS reference results.

5.2.1. Spatial averaged properties

Fig. 17 shows the temporal evolution of carrier phase kinetic energy, particle kinetic energy, and fluid-particle correlation. The carrier phase kinetic energy decreases due to viscous dissipation. Particle kinetic energy

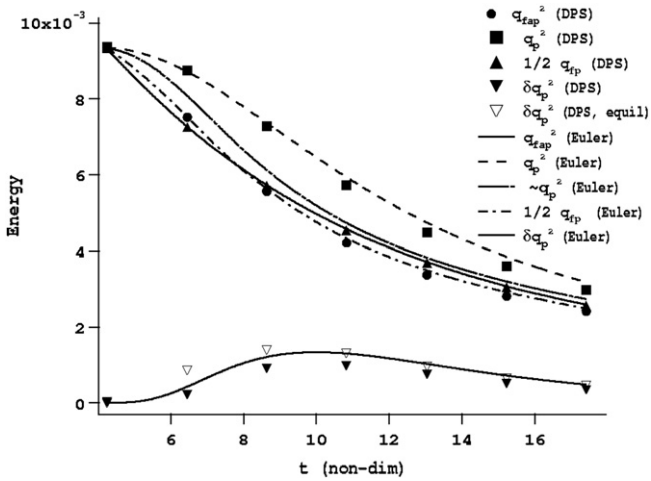

Fig. 17. Temporal evolution of the mean fluid, particle, and fluid-particle velocity correlations from DPS (symbols) and Eulerian simulations (lines). For the Eulerian approach the total particle kinetic energy q_p^2 is computed as the sum of the kinetic energy due to mesoscopic motion $\tilde{q}_p^2$ and the random uncorrelated energy δq_p^2. Case $St_K = 2.2$.

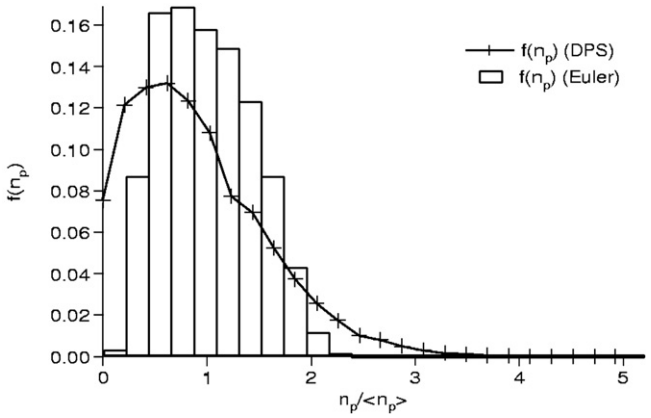

Fig. 18. Comparison of particle number density PDF measured from Lagrangian simulation with the one from mesoscopic Eulerian simulation. Case $St_K = 2.2$ at $t = 10.8$.

follows the carrier phase kinetic energy with a delay of the order of the particle relaxation time. Due to particle inertia, the particle velocities become partially uncorrelated in space and the RUE begins to increase. The behaviour of the integral quantities of mesoscopic and uncorrelated particle kinetic energy as well as the fluid-particle correlation are well predicted by the Eulerian simulation using the transport equation for RUE.

The RUE prediction is also compared to the empirical model of Février [7]. DPS performed in stationary homogeneous isotropic turbulence suggest that the mean uncorrelated kinetic energy δq_p^2 depends on the resolved dispersed phase kinetic energy $\breve{q}_p^2$, the fluid-particle correlation q_{fp}, and the carrier phase kinetic energy weighted by the particle presence $q_{f@p}^2 = 1/2\{u_k u_k\}_p$. This equilibrium expression is written,

$$\delta q_p^2 = \breve{q}_p^2 \left(\frac{4\breve{q}_p^2 q_{f@p}^2}{q_{fp}^2} - 1 \right) \tag{49}$$

After a transient time, mean RUE predicted by this model using DPS results are in good agreement with both Lagrangian and Eulerian results for non-dimensional time $t > 8.6$. This indicates that the flow is globally in equilibrium, in the sense that a model designed in stationary configuration works in this unsteady flow.

Comparison of particle number density PDF is provided on Fig. 18. As expected, the Eulerian approach underestimates particle segregation.

5.2.2. Instantaneous local mesoscopic fields

Fig. 19 shows a snapshot of number density in DPS and the Eulerian simulation in the upper and the lower graph. The number density field shows the same kind of structures for both the Lagrangian and Eulerian simulations. In contrast, the instantaneous distribution is less heterogeneous for the Eulerian simulation due to the heuristic bulk viscosity which reduces compressibility effects.

The heuristically introduced bulk viscous term tends to make the spatial particle number density more uniform. Without this bulk viscous term, Eulerian simulations can currently not be carried out: the physical particle segregation is too large as it could be resolved by the numerical scheme. Since the spatial average of the bulk viscosity term is however zero, it does not effect the temporal evolution of the mean kinetic energy of the random uncorrelated motion of the particles δq_p^2. In contrast, local instantaneous values of $\delta\breve{\theta}_p$ may differ notably from the values obtained in the DPS (Fig. 20).

5.3. Spectral kinetic energies

Fig. 21 shows spectra of the total kinetic energies of the dispersed phase as well as the compressible kinetic energies measured from the DPS and Eulerian simulation. First, one remarks the high compressible component of the kinetic energy compared to the gaseous carrier phase kinetic energy in the DPS results. This causes

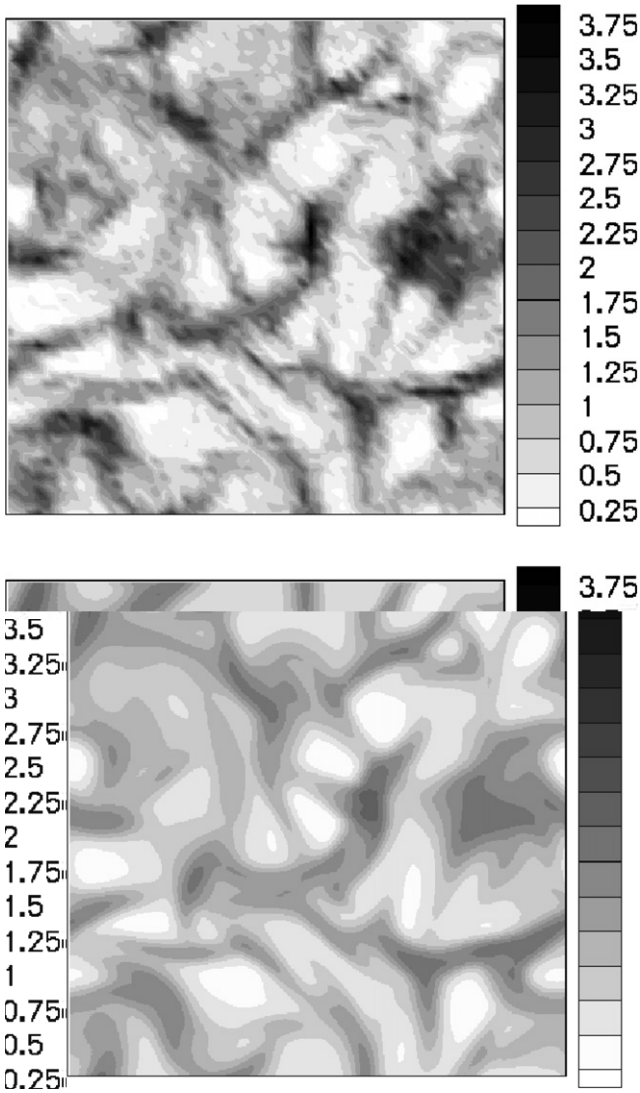

Fig. 19. Comparison of the normalized particle number density $\breve{n}_p/\langle\breve{n}_p\rangle$ measured from the Lagrangian simulation (upper graph, resolution 64^3) with the one given by the Eulerian simulation (lower graph, resolution 128^3) ($St_K = 2.2$) at time ($t = 10.8$). Same cut-plane as Fig. 15.

structures similar to those known as eddy shocklets in compressible turbulence [26]. In addition, the compressible part of the energy spectrum is of the same order than the solenoidal part at small scales or large wavenumber values. The kinetic energy spectrum of the Eulerian simulation does not reflect this behaviour to the same extend at small scales in contrast with the one measured at large scales or small wave number values. This discrepancy between both approaches is probably due to the bulk viscosity operator which reduces drastically the compressible effects at small scales.

6. Conclusion and perspectives

This study presents the numerical application of a new Eulerian approach for dispersed particles in turbulent flows based on a PDF approach conditioned by the fluid flow realization [1]. Comparison against Lagrangian simulation results are carried out for an ensemble of non-colliding particles suspended in a decaying homogeneous isotropic turbulence given by DNS. The proposed mesoscopic Eulerian approach allows to

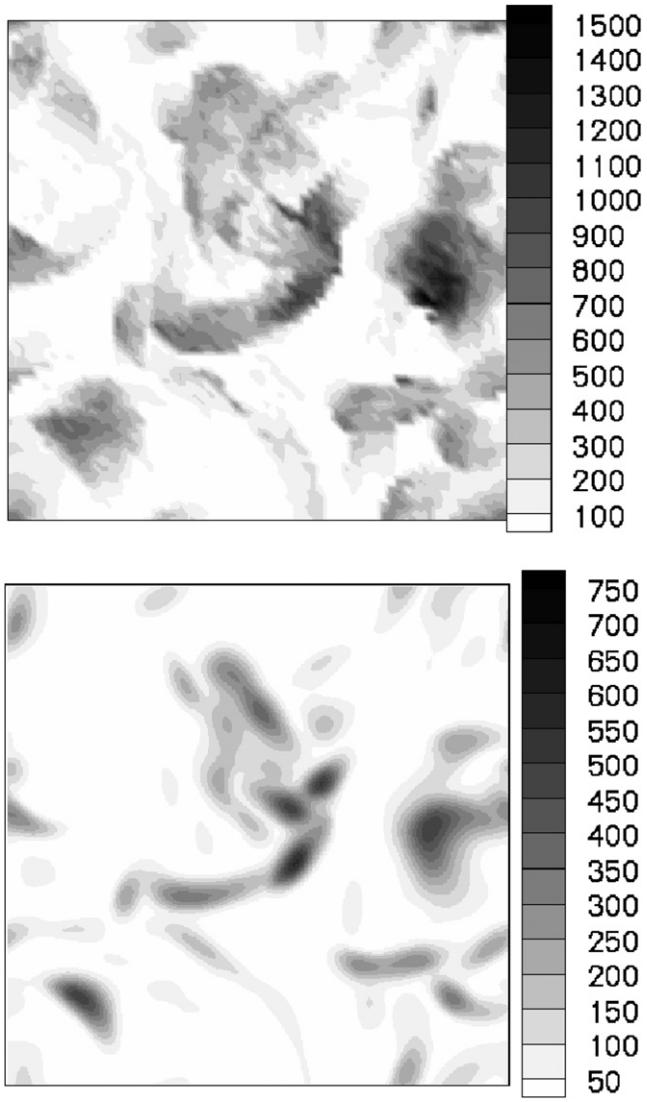

Fig. 20. Comparison of RUE ($\delta\breve{\theta}_p$) measured from the Lagrangian simulation (upper graph, resolution 64^3) with the one given by the Eulerian simulation (lower graph, resolution 128^3) after one particle relaxation ($St_K = 2.2$) time ($t = 10.8$). Same cut-plane as Fig. 15.

simulate the dynamics of inertial particles by accounting for the second-order moments of the particle velocity PDF in the momentum equation. Eulerian predictions of the time dependent particle and fluid-particle velocity correlations measured by spatial averaging in the whole computational domain are in good agreement with the Lagrangian simulation results. The compressible behaviour of the particle velocity field was pointed out, using the kinetic energy spectra measured from Eulerian and Lagrangian simulations. Such a behaviour, which is connected with the heterogeneous distribution of the particles, leads to peculiar difficulties for the numerical prediction of the mesoscopic Eulerian variables. These difficulties were overcome by adding a numerical bulk viscous term in the velocity transport equation which smooths artificially the local instantaneous particle number density distribution. In addition, simulations were performed at very small turbulent Reynolds numbers, because simulations with higher Reynolds numbers of the carrier phase are found to increase the numerical difficulties for the dispersed numerical predictions. Therefore, a more appropriate, less dispersive, numerical scheme is under development for the computation of the particle mesoscopic fields in order to remove the numerical bulk viscosity and to carry out simulations for higher Reynolds number values.

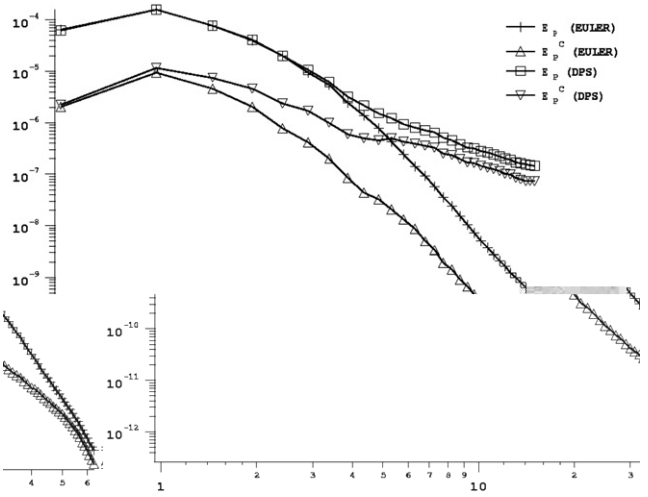

Fig. 21. Comparison of particle mesoscopic kinetic energy spectra computed from Lagrangian and Eulerian simulation results for Stokes number $St_K = 2.2$ at $t = 10.8$.

Concurrently, the mesocopic formalism is used for the development a Euler–Euler LES approach [27] for the unsteady computations of industrial turbulent two-phase flows loaded with particles or droplets.

Acknowledgments

Numerical computation of the Eulerian simulations were performed on the COMPAQ supercomputers of CEA and CERFACS. Numerical solutions on large grids (192^3, 256^3) were performed on SGI ORIGIN 3800 at CINES in the framework of the *Extreme Computing for Turbulent Combustion* program using up to 128 processors. The DPS reference solution was obtained with numerical simulations performed at computing center IDRIS using the DPS version of *NTMIX* in the *Ecoulements Reactifs Diphasiques: Simulations Directes et aux Grandes Echelles* project.

Financial support for this work was received from the European Community via the STOPP research training network.

References

[1] P. Février, O. Simonin, K.D. Squires, Partitioning of particle velocities in gas–solid turbulent flows into a continuous field and a spatially uncorrelated random distribution: theoretical formalism and numerical study, J. Fluid Mech. 533 (2005) 1–46.
[2] O. Druzhinin, S. Elghobashi, On the decay rate of isotropic turbulence laden with microparticles, Phys. Fluids 11 (3) (1999) 602–610.
[3] S.L. Rani, S. Balachandar, Evaluation of the equilibrium Eulerian approach for the evolution of particle concentration in isotropic turbulence, Int. J. Multiphase Flow 29 (2003) 1793–1816.
[4] B. Shotorban, S. Balachandar, Particle concentration in homogeneous shear turbulence simulated via Lagrangian and equilibrium Eulerian approaches, Phys. Fluids 18 (2006) 065105.
[5] S. Chapman, T. Cowling, The Mathematical Theory of Non-Uniform Gases, Cambridge Mathematical Library Edition., Cambridge University Press, 1939 (digital reprint 1999).
[6] O. Simonin, P. Février, J. Laviéville, On the spatial distribution of heavy particle velocities in turbulent flow: from continuous field to particulate chaos, J. Turbul. 3 (2002) 040.
[7] P. Février, Etude numerique des effets de concentration preferentielle et de correlation spatiale entre vitesses des particules solides en turbulence homogene isotrope stationaire, Ph.D. Thesis, INP Toulouse, France, 2000.
[8] M.W. Vance, K.D. Squires, O. Simonin, Properties of the particle velocity field in gas–solid turbulent channel flow, Phys. Fluids 18 (2006) 063302.
[9] M. Reeks, On a kinetic equation for the transport of particles in turbulent flows, Phys. Fluids A 3 (3) (1991) 446–456.
[10] O. Simonin, Combustion and turbulence in two phase flows, Lecture Series 1996-02, von Karman Institute for Fluid Dynamics, 1996.
[11] M. Sakiz, O. Simonin, Numerical experiments and modelling of non-equilibrium effects in dilute granular flows, in: Rarefied Gas Dynamics, in: R. Brun, R. Campargue, R. Gatignol, J.C. Lengrand (Eds.), Proceedings of the 21st International Symposium on Rarefied Gas Dynamics, July 1998, vol. 1, Cépaduès Editions, Marseille, France, 1999, pp. 287–294.

[12] S.B. Pope, Lagrangian pdf methods for turbulent flows, Annu. Rev. Phys. Mech. 26 (1994) 23–63.
[13] S. Elghobashi, G. Truesdell, On the two-way interaction between homogeneous turbulence and dispersed solid particles. I: turbulence modification, Phys. Fluids A 5 (7) (1993) 1790–1801.
[14] M. Boivin, O. Simonin, K.D. Squires, On the prediction of gas–solid flows with two-way coupling using large eddy simulation, Phys. Fluids 12 (2000) 2080–2090.
[15] O. Vermorel, B. Bedat, O. Simonin, T. Poinsot, Numerical study and modelling of turbulence modulation in a particle laden slap flow, J. Turbul. 335 (2003) 75–109.
[16] D.P. Schmidt, Theoretical analysis for achieving high-order spatial accuracy in Lagrangian/Eulerian source terms, Int. J. Numer. Methods Fluids 52 (8) (2006) 843–865.
[17] S. Elghobashi, G. Truesdell, Direct simulation of particle dispersion in a decaying isotropic turbulence, J. Fluid Mech. 242 (1992) 655–700.
[18] W. Snyder, J. Lumley, Some measurements of particle velocity autocorrelation functions in a turbulent flow, J. Fluid Mech. 48 (part 1) (1970) 41–71.
[19] T. Passot, A. Pouquet, Numerical simulation of compressible homogeneous flow in the turbulent regime, J. Fluid Mech. 181 (1987) 441–466.
[20] T. Schönfeld, M. Rudgyard, Steady and unsteady flows simulations using the hybrid flow solver AVBP, AIAA J. 37 (11) (1999) 1378–1385.
[21] S. Lele, Compact finite difference schemes with spectral like resolution, J. Comput. Phys. 103 (1992) 16–42.
[22] R. Kraichnan, An almost-Markovian Galilean-invariant turbulence model, J. Fluid Mech. 47 (1971) 513.
[23] A. Kaufmann, O. Simonin, T. Poinsot, J. Helie, Dynamics and dispersion in Eulerian–Eulerian DNS of two-phase flows, in: Proceedings of the Summer Program 2002, Studying Turbulence Using Numerical Simulation Databases IX, Center for Turbulence Research Stanford, CA, 2002, pp. 381–392.
[24] S.L. Rani, S. Balachandar, Preferential concentration of particles in isotropic turbulence: a comparison of the Lagrangian and equilibrium Eulerian approach, Powder Technol. 141 (2004) 109–118.
[25] A. Kaufmann, Towards Eulerian–Eulerian large eddy simulation of reactive two-phase flows, Ph.D. Thesis, INP Toulouse, France, 2004.
[26] G. Erlebacher, M.Y. Hussaini, C.S.T. Zang, Toward the large eddy simulation of compressible turbulent flows, ICASE 90–76 (1990) 1–43.
[27] M. Moreau, B. Bedat, O. Simonin, A priori testing of subgrid stress models for Euler–Euler two-phase LES from Euler–Lagrange simulations of gas-particle turbulent flow, in: 18th Ann. Conf. on Liquid Atomization and Spray Systems, ILASS Americas, 2005.